IEEE TRANS. ANTENNAS AND PROPAGATION, vol. 68, no. 9, pp. 6826-6831, Sept. 2020, DOI: 10.1109/TAP.2020.2975617

Broadband Linear-to-Circular Polarizing Reflector for Space Applications in Ka-Band

Eduardo Martinez-de-Rioja, Jose A. Encinar, Antonio Pino, and Yolanda Rodriguez-Vaqueiro

***Abstract*—This communication presents a novel low-profile broadband polarizing reflector to convert dual linear polarization (LP) into dual circular polarization (CP). The polarizing cell is based on printed dipole technology and presents a wideband performance in Ka-band. The dimensions of the printed dipoles are adjusted cell by cell to improve the reflection phase performance against variations in the incidence angles or in the cell dimensions. A 25-cm flat polarizing reflector demonstrator has been designed, fabricated and tested. The design has been optimized for transmit (19.2-20.2 GHz) and receive (29-30 GHz) frequencies in Ka-band, but the broadband behavior of the cell provides satisfactory results also at the intermediate frequencies. The measured patterns show a good agreement with the simulations, with an axial ratio lower than 1.8 dB within the 19.2-30 GHz band. The proposed polarizing reflector can be used for novel multibeam antenna configurations to produce multi-spot coverage in Ka-band with a smaller number of apertures.**

***Index Terms*—Polarizing reflector, dual polarization, circular polarization, multibeam antennas, satellite communications.**

I. Introduction

The design of polarizing reflective surfaces has attracted an increased interest over the last years, due to their applications in multiple beam antenna (MBA) systems for communication satellites in Ka-band. Current MBAs typically employ four reflector apertures operating in a single feed per beam (SFPB) basis to provide cellular coverage at transmit (Tx) and receive (Rx) frequencies in Ka-band, exploiting frequency and polarization reuse to increase the system capacity [1]-[2]. A significant effort has been done to reduce the number of antennas required to produce the complete coverage [3]-[9]. Some of the proposed MBA concepts, such as multiple feed per beam (MFPB) architectures [3], direct radiating arrays [4] and active lenses [5] have the drawbacks of higher complexity and cost than standard SFPB reflector technology. Reflectarray antennas have been investigated to generate two spaced beams per feed in orthogonal circular [6] or linear [7]-[8] polarization (CP, LP), but a further effort is required to demonstrate their capability to fulfill the stringent requirements of satellite MBAs.

One attractive solution to produce adjacent spots in right-hand and left-hand CP (RHCP, LHCP) that keeps SFPB operation is based on two dual-reflector systems with a polarization selective subreflector (PSS) [9]. The PSS allows to combine two separate feed clusters operating in orthogonal polarization, so that only two main apertures are required to produce a four-color multispot coverage for Tx and Rx in Ka-band. The two antennas can be accommodated in one of the lateral faces of the satellite, with a substantial reduction in volume and weight compared to the standard four-reflector configuration [9]. One possible implementation of the dual-reflector system is based on a CP selective subreflector illuminated by dual-band CP feeds. CP selective surfaces based on multi-layer meander line designs [10]-[11] have been proposed to be used as PSS, but they require a large number of stacked layers. A two-layer CP selective surface has been shown in [12], but it provides limited bandwidth. On the other hand, the use of an LP selective subreflector (e. g., a dual-gridded reflector [13] or a flat reflectarray [14]-[15]) illuminated by dual-band LP feeds reduces the design complexity of the PSS, although it requires a polarizing main reflector to convert dual-LP into dual-CP at both Tx and Rx frequencies [9].

Several works have been reported on the design of linear-to-circular polarizing reflective surfaces based on periodic arrays of printed elements [16]-[19]. Broadband polarizing surfaces were demonstrated in Ku-band [16], showing a 3-dB axial ratio relative bandwidth of around 60%. In [17], a dual-band polarizing reflective surface was shown to provide orthogonal CP in Tx and Rx bands, but the large unit-cell dimensions can lead to the appearance of grating lobes. The dual-band polarizing cell presented in [18] avoids this problem, as it exhibits a period lower than $\lambda/2$. Recently, a single-layer polarizer operating in reflection was designed and demonstrated [19], showing a conversion from dual-LP into dual-CP from 20 to 30 GHz with low axial ratio (less than 2 dB) for angles of incidence of up to 20º; however, the axial ratio increases for larger angles of incidence. Polarizing surfaces in transmission mode typically require a larger number of layers than their reflection counterparts [19]-[21]. A dual-band transmission polarizer has been recently demonstrated in [22] using three layers. In all the previous works, the geometry of the polarizing cell is adjusted for specific incidence and periodicity conditions, and then the cell is replicated to form a periodic array of elements. In [23], some aperiodic adjustments were introduced in the cells of the polarizing surface to reduce the cross-polarization.

In this paper, the authors propose a novel low-profile broadband polarizing reflector to convert dual-LP into dual-CP. The polarizing cell is based on printed dipole technology and presents a wideband performance in Ka-band (a relative bandwidth larger than 50% with an axial ratio less than 2 dB). The dimensions of the dipoles on each cell are adjusted to provide an improved performance and compensate the variations in the incidence angles or in the cell dimensions between neighbor cells. A 25-cm flat polarizing reflector prototype has been fabricated and measured in order to demonstrate the proposed concept for LP-to-CP conversion. This technology can be used to design the main reflector of a dual-reflector configuration

This work has been supported in part by the Spanish Ministry of Economy and Competitiveness and the European Regional Development Fund, under Projects TEC2016-75103-C2-1-R and TEC2015-65353-R, and in part by the European Space Agency ESTEC under Contract 4000117113/16/NL/AF.

E. Martinez-de-Rioja is with the Department of Signal Theory and Communications and Telematic Systems and Computing, Universidad Rey Juan Carlos, 28942 Madrid, Spain (e-mail: eduardo.martinez@urjc.es).

J. A. Encinar is with the Information Processing and Telecommunications Center, Universidad Politécnica de Madrid, 28040 Madrid, Spain (e-mail: jose.encinar@upm.es).

A. Pino and Y. Rodriguez-Vaqueiro are with the Department of Signal Theory and Communications, Universidad de Vigo, 36310 Vigo, Spain (e-mail: agpino@com.uvigo.es; yrvaqueiro@com.uvigo.es).

as the one shown in Fig. 1, where the subreflector is a dual-band reflectarray illuminated by a cluster of feeds radiating in dual-LP. The reflectarray subreflector will be able to provide independent phase adjustment in each LP at both Tx and Rx, through the use of reflectarray cells as those presented in [14]-[15]. This will allow to deviate the RHCP and LCHP beams produced by the main reflector in opposite directions, changing the sign of the deviation between the Tx and Rx bands in order to produce orthogonal spots at Tx and Rx, as it is typically required for multispot coverages in Ka-band [2].

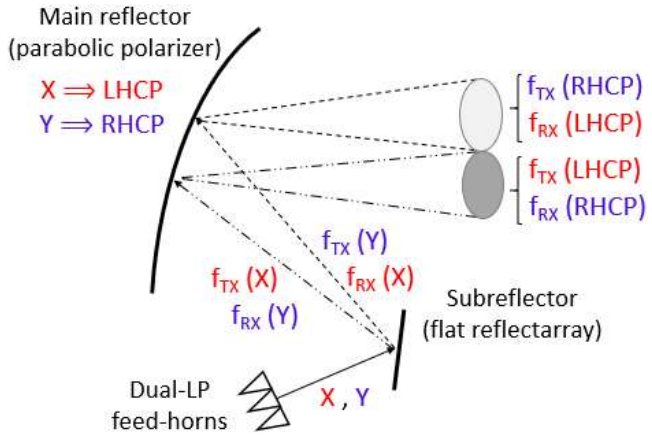

Fig. 1 Dual-reflector configuration to produce multiple beams in dual-CP, formed by a flat reflectarray subreflector and a parabolic polarizing reflector.

II. Broadband Polarizing Cell

The polarizing cell consists of three parallel dipoles placed forming an angle of 45º with respect to the *x*-axis in the absolute reference system of the cell, as shown in Fig. 2(a). The dipoles are characterized by their length (L_i), width (w_i) and separation (S). The lateral dipoles have the same dimensions, in order to reduce the cross-polar components by keeping the symmetry with respect to the central dipole. The cell is composed of two dielectric layers, see Fig. 2(b). The upper dielectric is a Rogers Rflex3000 flexible substrate, with thickness h_B = 0.05 mm and electrical properties ε_{rB} = 2.9 and $\tan\delta_B$ = 0.0025. This layer acts as a protective coat (the dipoles would be printed on its inner side) and it will be bonded to a foam of thickness h_A = 3 mm (Divinycell-HT81, with ε_{rA} = 1.09 and $\tan\delta_A$ = 0.0005), which is backed by the ground plane. Note that a second reference system (*x*' and *y*' axes) has been defined by 45º rotation in the *xy*-plane of the absolute *x* and *y* axes. The definition of the incidence angles on the cell (θ_i , φ_i) is depicted in Fig. 2(c).

The operating principle of the polarizing cell can be explained as follows. Assuming a linearly polarized wave with the electric field in the direction of the *x*-axis that strikes at normal incidence the periodic cell, the incident electric field can be decomposed into two orthogonal components of the same amplitude, one in the direction of the positive *x*'-axis and the other in the direction of the negative *y*'-axis, as shown in Fig. 3(a). The geometrical parameters of the cell (dipole lengths, widths, etc.) can be adjusted to provide 90º difference between the phase of the reflected *x*'-component (controlled by the dipoles) and the phase of the reflected *y*'-component (orthogonal to the dipoles, so it will be reflected by the ground plane). The same applies when the incident field is oriented in the direction of the *y*-axis, and two orthogonal components in the directions of the positive *x*' and *y*' axes are obtained, see Fig. 3(b). Thus, if the requirement of introducing 90º phase shift between *x*' and *y*' components is fulfilled, the reflected field will be circularly polarized, being RHCP or LHCP depending on the polarization of the incident field. This principle can be applied in the same way for a wave striking at oblique incidence.

The reason for using three dipoles is to provide more degrees of freedom for the design of the polarizing reflector. The lengths of the dipoles on each cell will be adjusted to compensate the effect of variations in the incidence angles or in the cell dimensions (which is not the case of a flat polarizing surface, but it is significant in a parabolic reflector, as the one shown in Fig. 1) in the cell response, in order to keep the 90º phase shift between the reflected *x*' and *y*' components. Also, the three-dipole cell provides a broadband response of the phase difference curve, as will be shown later.

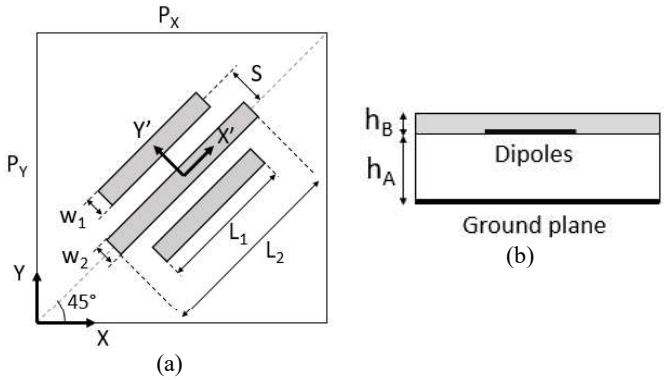

Fig. 2 Upper (a) and lateral (b) views of the polarizing cell, which consists of three coplanar parallel dipoles placed with 45º slant with respect to the *x*-axis.

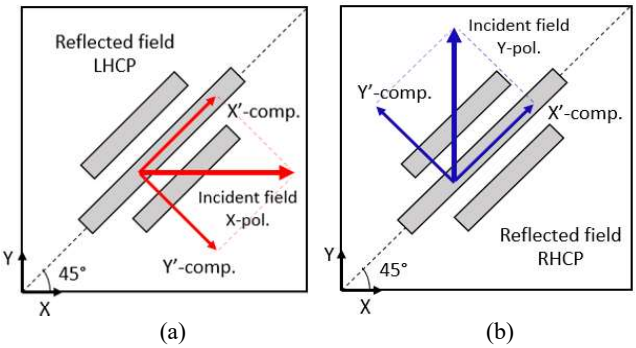

Fig. 3 Concept for converting dual-LP into dual-CP: (a) with the incident electric field in the direction of the x-axis, and (b) with the incident electric field in the direction of the y-axis.

The geometrical parameters of the cell have been adjusted to provide 90º phase difference between the reflected *x*' and *y*' components of the electric field at both Tx (19.2-20.2 GHz) and Rx (29-30 GHz) frequencies in Ka-band, considering oblique incidence conditions (θ_i = 20º, φ_i = 0º). The dimensions of the cell have been set to $P_X = P_Y$ = 5 mm (which is 0.5λ at 30 GHz), in order to avoid the appearance of grating lobes at the higher frequencies. The values selected for the dipole dimensions are as follows: L_1 = 3.2 mm, w_1 = 0.4 mm, L_2 = 4 mm, w_2 = 0.6 mm, S = 1.1 mm. Fig. 4 shows the amplitude and phase of the reflection coefficients associated to the linear components in the rotated reference system (*x*' and *y*') for the polarizing cell designed with the previous parameters under θ_i = 20º, φ_i = 0º incidence. The cell has been analyzed using an in-house Method of Moments in the Spectral Domain (SD-MoM) code [24] and assuming it is placed in a periodic environment. The SD-MoM simulations have been validated using the commercial software CST Microwave Studio [25], and both results are included in Fig. 4. As can be seen, there is a quite good agreement between the curves obtained by the SD-MoM code and by CST. The amplitude of the reflection coefficients associated to the *x*' and *y*' components is less than 0.03 dB for frequencies below 31 GHz (the simulations account

for the dielectric losses of the substrates; the conductivity losses of the copper are almost negligible at these frequencies). The amplitude of the cross-polar coefficients is lower than -20 dB within the 17-32 GHz band. The difference between the phases of the co-polar reflection coefficients presents a steady response within the 18-31 GHz band, with values close to -90º. The geometrical parameters of the polarizing cell have been adjusted to achieve exactly -90º at 19.7 and 29.5 GHz (central frequencies for Tx and Rx in Ka-band), but the broadband performance of the cell allows to obtain very good results also at the intermediate frequencies.

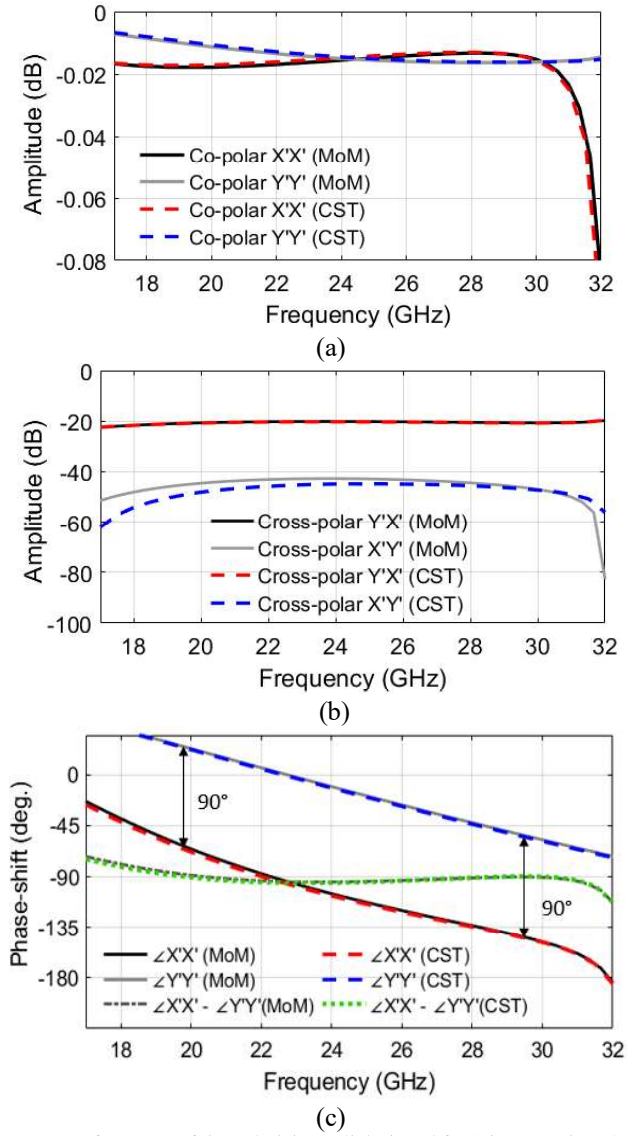

Fig. 4 Performance of the polarizing cell designed for (θi = 20º, φi = 0º): amplitude of the (a) co-polar and (b) cross-polar reflection coefficients associated to the *x*' and *y*' components, (c) phase of the co-polar reflection coefficients and difference between them.

Fig. 5 shows in solid lines the variation in the phase difference between the reflected *x*' and *y*' components for different values of the incidence angle θ_i and the cell period P_X, considering the lengths of the dipoles previously designed for θ_i = 20º, φ_i = 0º and P_X = 5 mm (named as design A). It can be observed that the variation of the previous parameters has a negative impact on the performance of the polarizing cell, leading to significant errors with respect to the required -90º phase difference, especially at 30 GHz. To overcome this problem, the lengths of the dipoles have been adjusted by means of a dual-frequency optimization technique to maintain the -90º phase at both 19.7 and 29.5 GHz. The dipole lengths resulting from the optimization are as follows: 1) L_1 = 2.975 mm and L_2 = 4.25 mm for the case with θ_i = 0º and P_X = 5 mm (design B), 2) L_1 = 2.9 mm and L_2 = 4.2 mm for θ_i = 10º and P_X = 4.75 mm (design C), and 3) L_1 = 3.54 mm and L_2 = 3.65 mm for θ_i = 28º and P_X = 5.3 mm (design D). The phase difference curves obtained after the optimization of the dipole lengths have been included in Fig. 5, in dashed lines.

The axial ratio of the reflected RHCP and LHCP has been depicted in Fig. 6, considering different designs of the dipoles (A, B C and D) and their associated incidence angles and cell dimensions. The cell presents a broadband performance within the 18-31 GHz band, where the axial ratio is below 2 dB (a relative bandwidth of 53%). An axial ratio less than 1.3 dB can be achieved within the same frequency band for angles of incidence up to θ_i = 20º. The lowest values of axial ratio (<1 dB) in all the cases studied correspond to frequencies around 19.7 and 29.5 GHz, which are the two frequencies where the -90º phase difference condition has been enforced.

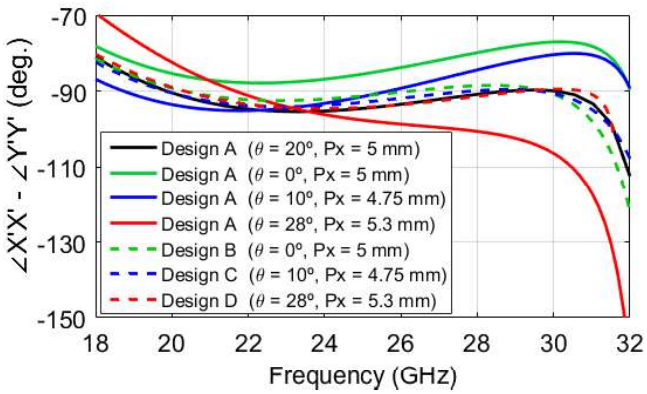

Fig. 5 Difference between the phases of the reflected *x*' and *y*' components for different angles of incidence and cell dimensions, considering four different designs of the dipoles (A, B, C and D).

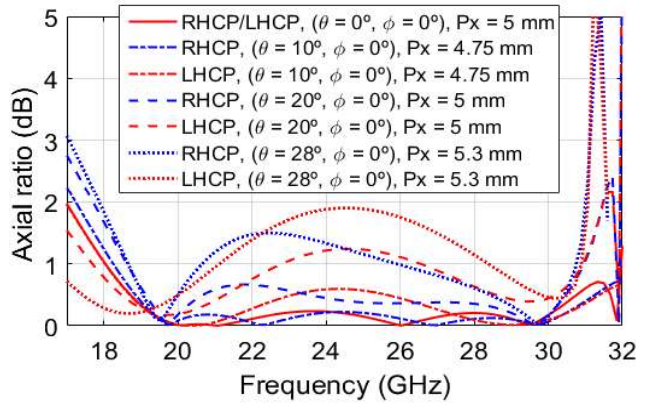

Fig. 6 Axial ratio provided by the polarizing cell for the reflected RHCP and LHCP waves, considering different dimensions of the dipoles (designs A, B, C and D) and their associated incidence and periodicity conditions.

III. Experimental Validation

A 25-cm flat polarizing reflector demonstrator has been designed, manufactured and tested in order to validate the proposed concept for broadband dual-LP to dual-CP conversion in Ka-band (see Fig. 7). The prototype consists of a rectangular array of 54 x 54 cells, where the lengths of the dipoles on each cell have been adjusted to provide 90º phase shift between the orthogonal linear components of the reflected field, accounting for the real incidence angles from the feed. The design of the dipoles has been optimized for Tx (19.2-20.2 GHz)

Citation information: DOI 10.1109/TAP.2020.2975617

and Rx (29-30 GHz) frequencies in Ka-band, but the broadband performance of the polarizing cell will allow to obtain satisfactory results also at the intermediate frequencies, as will be shown latter.

The lower dielectric layer is a 3-mm foam (Rohacell 51-HF) with electrical properties ε_{rA} = 1.08 and $\tan\delta_A$ = 0.0021, and the upper layer is a flexible substrate of 50 μm thickness (DSflex 600) with ε_{rB} = 3.2 and $\tan\delta_B$ = 0.005. The dipoles have been photo-etched on the inner side of the DSflex 600 sheet, and then, the substrate has been bonded to the foam using 3M Adhesive Tape 927. The same adhesive has been used to bond the other side of the foam to the copper ground plane. The two layers of adhesive tape (ε_r = 3.21, $\tan\delta$ = 0.04 and 50 μm thickness) have been considered in the design of the dipoles.

The 25-cm flat polarizing reflector has been illuminated using a Ka-band horn of 60-mm diameter, which is placed in an offset configuration, see Fig. 7. The feed is located 43 cm away from the polarizer along the *z*-axis (vertical axis), with an offset of 12 cm in the direction of the *x*-axis, so that it illuminates the reflectarray center with an angle of 15.5º. This feed position was chosen to avoid blockage of the beam, which is radiated in the specular direction of the feed (θ_b = 15.5º in the *xz*-plane). Note that the polarizing reflector does not collimate the beam, as it only converts the incident LP from the feed in reflected CP. The subtended angle from the feed on the 25-cm polarizer is 31º, which results in around -11 dB edge illumination at the lowest frequency (19.2 GHz).

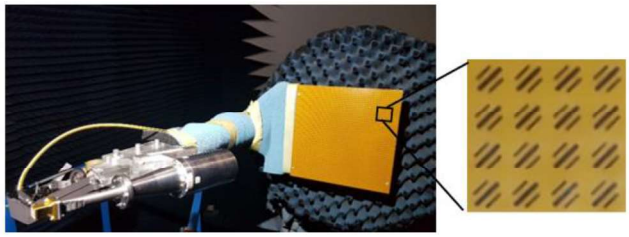

Fig. 7 Picture of the prototype in the anechoic chamber and detail of the printed dipoles.

The simulated radiation patterns of the designed polarizer in the *xz*-plane for LHCP at 19.7 GHz and 29.5 GHz (central frequencies of the Tx and Rx bands) are shown in Fig. 8. The results for RHCP are not included in Fig. 8 since they are very similar. A conventional $\cos^q(\theta)$ function has been used to simulate the radiation patterns of the horn. The value of 'q' at each frequency has been estimated based on electromagnetic simulations provided by the manufacturer of the horn [26], resulting in q = 35 at 19.7 GHz and q = 63 at 29.5 GHz. In order to evaluate the performance of the linear-to-circular polarization conversion, additional simulations have been carried out by eliminating the dipoles and computing the radiation patterns in dual-LP obtained by direct reflection in the copper ground plane (note that the two dielectric layers placed above the ground plane are still considered in the simulations, but not the dipoles). The results for X-polarization have been included in the patterns shown in Fig. 8. The reduction in the gain of the co-polar components for LHCP and RHCP with respect to the linear polarized beams reflected by the ground plane (X and Y) is lower than 0.1 dB, while the cross-polar levels for RHCP and LHCP are several dB higher than in the LP case, as a consequence of the polarization conversion. Despite this fact, the cross-polar components of each CP are more than 25 dB below the co-polar maximum at both operating frequencies (axial ratio < 1 dB).

The fabricated demonstrator has been tested at the anechoic chamber of the Universidad Politécnica de Madrid, in a compact-range measurement system. The radiation patterns of the polarizing reflector in the *xz*-plane and in the orthogonal plane forming 15.5º with the *z*-axis (azimuth) have been measured at several frequencies ranging from 19.2 to 30 GHz. The results for LHCP are presented in Fig. 9 (note that very similar results are obtained for RHCP).

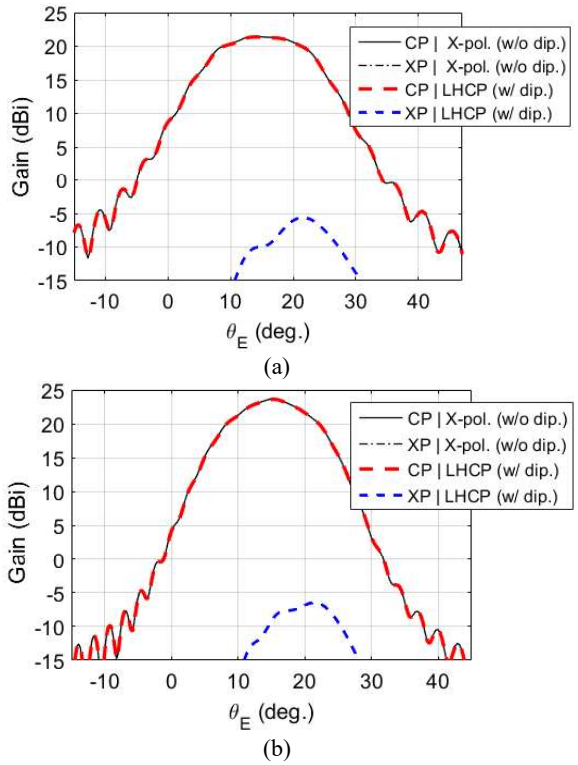

Fig. 8 Comparison of simulated radiation patterns for the designed polarizer with printed dipoles (radiating in CP) and without dipoles (radiating in LP) in the xz-plane: (a) at 19.7 GHz and (b) at 29.5 GHz.

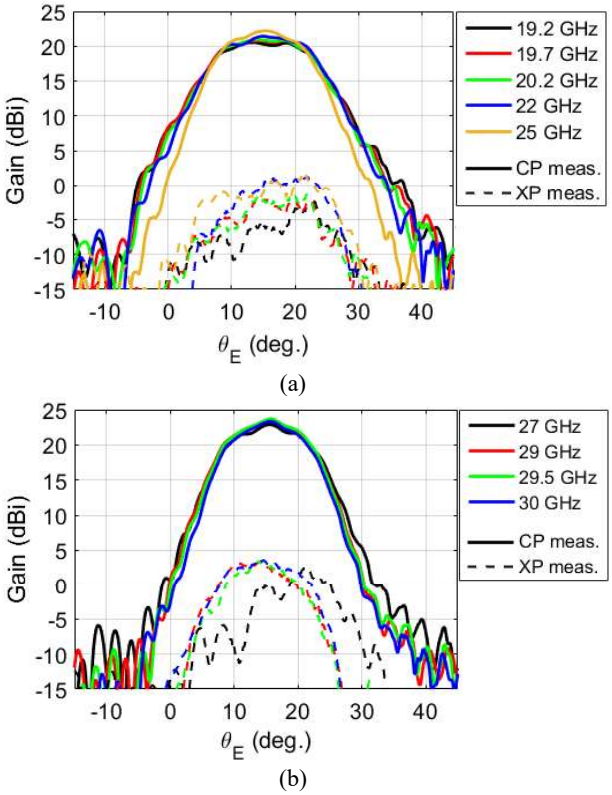

Fig. 9 Superposition of measured radiation patterns in LHCP (xz-plane): (a) frequencies from 19.2 to 25 GHz and (b) frequencies from 27 to 30 GHz.

Citation information: DOI 10.1109/TAP.2020.2975617

Since the polarizing reflector only converts the incident dual-LP into reflected dual-CP, the gain and beamwidth of the measured co-polar patterns shown in Fig. 9 are determined by the feed-horn, which is more directive at the higher frequencies. The measured cross-polar levels are greater than in the initial simulations, varying between -23 dB (at the lower frequencies) and -20 dB (at the higher frequencies) with respect to the co-polar maximum. This can be checked by comparison with the simulated patters shown in Fig. 8, where the maximum cross-polar levels at 19.7 and 29.5 GHz are around -25 dB and -30 dB, respectively.

Several factors were investigated as potential causes that can deteriorate the cross-polar patterns: variations in the electrical properties of the dielectrics, feed positioning, manufacturing tolerances, etc. Finally, it was checked that the cross-polar increase was mainly produced by the variation in the thickness of the foam sheet (from 3 mm to 2.85 mm) during the manufacturing of the prototype, as a consequence of the bonding process with the upper dielectric and the ground plane. This reduction in the foam thickness has a negative impact on the performance of the polarizing cell, leading to higher cross-polar levels. This fact was taken into account in the simulations of the 25-cm polarizer, resulting in a quite better agreement with the measurements, as can be seen in Figs. 10 and 11 for the RHCP patterns at 19.7 GHz and 29.5 GHz, respectively (the results are very similar for both CP, so only RHCP is shown). It can be observed a small ripple in some of the patterns, which is mainly due to diffraction effects in the edges of the 25-cm panel and to small inaccuracies in the measurement experimental setup. Apart from the small discrepancies caused by these factors, a quite good matching has been obtained between simulated and measured patterns.

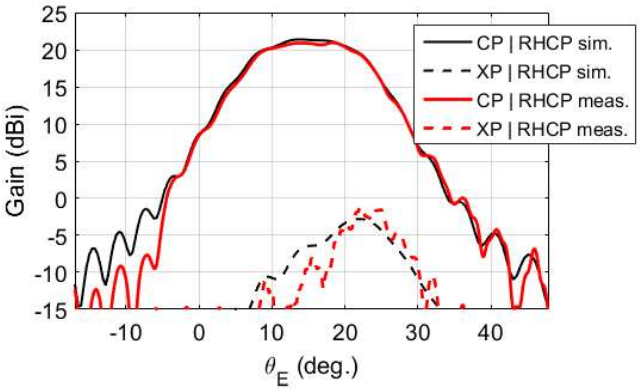

Fig. 10 Comparison of measurements and corrected simulations for the radiated RHCP at 19.7 GHz in the (a) xz-plane and (b) azimuth plane.

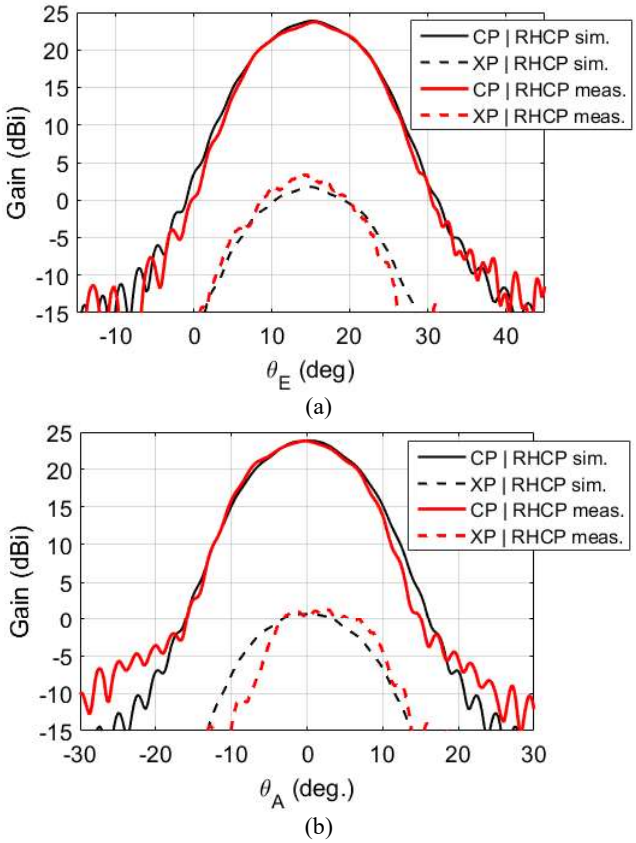

Fig. 11 Comparison of measurements and corrected simulations for the radiated RHCP at 29.5 GHz in the (a) xz-plane and (b) azimuth plane.

The measured cross-polar levels at different frequencies in Ka-band (from 19.2 GHz to 30 GHz, a relative bandwidth of 45%) are between -23 dB and -20 dB below the co-polar for both RHCP and LHCP, which leads to an axial ratio between 1.23 dB and 1.74 dB, see Fig. 12. These results could be improved by a more careful fabrication of the polarizing reflector. If the variation in the foam thickness is kept below ±0.055 mm, the axial ratio will be less than 1 dB within the same frequency band, as it is shown in Fig. 12 for the initial simulations of the 25-cm flat polarizing reflector with a 3-mm thick foam. These results demonstrate the proposed concept for a broadband polarizing reflector that is able to transform dual-LP into dual-CP, covering both downlink and uplink frequencies in Ka-band.

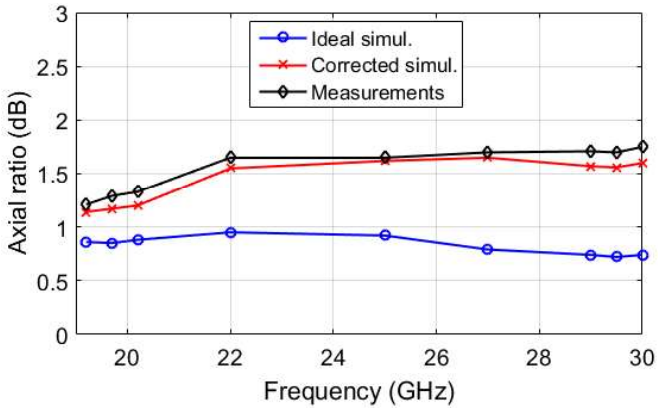

Fig. 12 Axial ratio versus frequency for the 25-cm flat polarizer demonstrator, comparing measurements, initial simulations (with a foam thickness of 3 mm) and corrected simulations (with a foam thickness of 2.85 mm).

IV. Conclusion

A broadband linear-to-circular polarizing reflector has been proposed and validated. The polarizing cell is composed of three coplanar parallel dipoles placed with 45º slant with respect to the direction of the normally-incident LP waves. The element provides around 50% relative bandwidth for an axial ratio lower than 2 dB under different incidence and periodicity conditions. The proposed cell has been used to design a 25-cm flat polarizing reflector demonstrator, for operation at Tx and Rx frequencies in Ka-band. An optimization procedure based on adjusting the lengths of the dipoles on each cell has been implemented to compensate variations in the cell response produced by the changes in the incidence angles and/or in the cell dimensions. The radiation patterns of the demonstrator have been measured at different frequencies in Ka-band (from 19.2 to 30 GHz), showing a quite good matching with the simulations. The polarizing cells and the optimization technique demonstrated here can be directly applied to design a parabolic polarizing reflector to generate adjacent beams in orthogonal CP for communication satellites in Ka-band.

References

[1] M. Schneider, C. Hartwanger and H. Wolf, “Antennas for multiple spot beams satellites”, CEAS Space Journal, Vol. 2, pp. 59-66, Dec. 2011.

[2] H. Fenech, S. Amos, A. Tomatis, and V. Soumpholphakdy, "High throughput satellite systems: An analytical approach," *IEEE Trans. Aerosp. Electron. Syst.*, vol. 51, no. 1, pp. 192-202, Jan. 2015.

[3] M. Schneider, C. Hartwanger, E. Sommer, H. Wolf, “Test results for the multiple spot beam antenna project Medusa”, in *Proc. 4th Eur. Conf. Antennas Propag. (EuCAP)*, Barcelona, Spain, Apr. 2010.

[4] O. M. Bucci, T. Isernia, S. Perna and D. Pinchera, “Isophoric sparse arrays ensuring global coverage in satellite communications”, *IEEE Trans. Antennas Propag.*, vol. 62, no. 4, pp. 1607-1618, Apr. 2014.

[5] G. Ruggerini, G. Toso and P. Angeletti, “An aperiodic active lens for multibeam satellite applications: From the design to the breadboard manufacturing and testing”, in *Proc. 5th Eur. Conf. Antennas Propag. (EuCAP)*, Rome, Italy, Apr. 2011, pp. 3697-3701.

[6] M. Zhou and S. B. Sørensen, "Multi-spot beam reflectarrays for satellite telecommunication applications in Ka-band", *10th Eur. Conf. Antennas Propag. (EuCAP)*, Davos, Switzerland, Apr. 2016, pp.1-5.

[7] D. Martinez-de-Rioja, E. Martinez-de-Rioja, J. A. Encinar, R. Florencio and G. Toso, "Reflectarray to generate four adjacent beams per feed for multispot satellite antennas", *IEEE Trans. Antennas Propag.*, vol. 67, no. 2, pp. 1265-1269, Feb. 2019.

[8] E. Martinez-de-Rioja, J. A. Encinar, R. Florencio and C. Tienda, "3-D bifocal design method for dual-reflectarray configurations with application to multibeam satellite antennas in Ka-band", *IEEE Trans. Antennas Propag.*, vol. 67, no. 1, pp. 450-460, Jan. 2019.

[9] N. J. G. Fonseca and C. Mangenot, “Low-profile polarizing surface with dual-band operation in orthogonal polarizations for broadband satellite applications,” in *Proc. 8th Eur. Conf. Antennas Propag. (EuCAP)*, The Hague, Netherlands, Apr. 2014, pp. 471–475.

[10] M.-A. Joyal and J.-J. Laurin, “Design and analysis of a cascade circular polarization selective surface at K band,” *IEEE Trans. Antennas Propag.*, vol. 62, no. 6, pp. 3043–3053, Jun. 2014.

[11] J. Lundgren, A. Ericsson and S. Sjoberg, “Design, optimization and verification of a dual band circular polarization selective structure”, *IEEE Trans. Antennas Propag.*, vol. 66, no. 11, pp. 6023-6032, Nov. 2018.

[12] W. Tang, G. Goussetis, N. J. G. Fonseca, H. Legay, E. Saenz and P. de Maagt, “Coupled split-ring resonator circular polarization selective surface”, *IEEE Trans. Antennas Propag.*, vol. 65, no. 9, pp. 4664-4675, Sept. 2017.

[13] M. Baunge, H. Ekstrom, P. Ingvarson and M. Petersson, “A new concept for dual gridded reflectors”, in *Proc. 4th Eur. Conf. Antennas Propag. (EuCAP)*, Apr. 2010, pp. 1-5.

[14] E. Martinez-de-Rioja, J. A. Encinar, R. Florencio and R. R. Boix, “Reflectarray in K and Ka bands with independent beams in each polarization”, in *Proc. IEEE Antennas Propag. Soc. Int. Symp.*, Fajardo, PR, USA, July 2016, pp. 1199-1200.

[15] E. Martinez-de-Rioja, J. A. Encinar, M. Barba, R. Florencio, R. R. Boix and V. Losada, “Dual polarized reflectarray transmit antenna for operation in Ku- and Ka-bands with independent feeds”, *IEEE Trans. Antennas Propag.*, vol. 65, no. 6, pp. 3241-3246, June 2017.

[16] E. Doumanis, G. Goussetis, J. L. Gomez-Tornero, R. Cahill and V. Fusco, "Anisotropic impedance surfaces for linear to circular polarization conversion", *IEEE Trans. Antennas Propag.*, vol. 60, no. 1, pp. 212-219, Jan. 2012.

[17] N. J. G. Fonseca and C. Mangenot, “High-performance electrically thin dual-band polarizing reflective surface for broadband satellite applications”, *IEEE Trans. Antennas Propag.*, vol. 64, no. 2, pp. 640-649, Feb. 2016.

[18] W. Tang, S. Mercader-Pellicer, G. Goussetis, H. Legay, N. J. G. Fonseca, “Low-profile compact dual-band unit cell for polarizing surfaces operating in orthogonal polarizations”, *IEEE Trans. Antennas Propag.*, vol. 65, no. 3, pp. 1472-1477, Mar. 2017.

[19] G. Perez-Palomino *et al.*, "A design technique based on equivalent circuit and coupler theory for broadband linear to circular polarization converters in reflection or transmission mode", *IEEE Trans. Antennas Propag.*, vol. 66, no. 5, pp. 2428-2438, May 2018.

[20] M. Hosseini and S. V. Hum, “A circuit-driven design methodology for a circular polarizer based on modified Jerusalem cross grids”, *IEEE Trans. Antennas Propag.*, vol. 65, no. 10, pp. 5322–5331, Oct. 2017.

[21] S. M. A. M. H. Abadi and N. Behdad, “Wideband linear-to-circular polarization converters based on miniaturized-element frequency selective surfaces”, *IEEE Trans. Antennas Propag.*, vol. 64, no. 2, pp. 525–534, Feb. 2016.

[22] P. Naseri, S. A. Matos, J. R. Costa, C. A. Fernandes and N. J. G. Fonseca, “Dual-band dual-linear-to-circular polarization converter in transmission mode application to K/Ka-band satellite communications”, *IEEE Trans. Antennas Propag.*, vol. 66, no. 12, pp. 7128–7137, Dec. 2018.

[23] S. Mercader-Pellicer, G. Goussetis, G. M. Medero, H. Legay, D. Bresciani and N. J. G. Fonseca, “Cross-polarization reduction of linear-to-circular polarizing reflective surfaces”, *IEEE Antennas Wireless Propag. Lett.,* vol. 18, no. 7, pp. 1527-1531, Jul. 2019.

[24] R. Florencio, J. A. Encinar, R. R. Boix, V. Losada, and G. Toso, “Reflectarray antennas for dual polarization and broadband telecom satellite applications,” *IEEE Trans. Antennas Propag.*., vol. 63, no. 4, pp. 1234-1246, Apr. 2015.

[25] CST Microwave Studio, Computer Simulation Technology [Online]. Available: *www.cst.com*

[26] ANTERAL: https://www.anteral.com/en.